Published in final edited form as:
J Control Release. 2012 March 10; 158(2): 319–328. doi:10.1016/j.jconrel.2011.10.028.

Photothermal-Chemotherapy with Doxorubicin-Loaded Hollow Gold Nanospheres: A Platform for Near-Infrared Light-Trigged Drug Release

Jian You[a,b], **Rui Zhang**[b], **Guodong Zhang**[b], **Meng Zhong**[b], **Yang Liu**[b], **Carolyn S. Van Pelt**[c], **Dong Liang**[d], **Wei Wei**[e], **Anil K. Sood**[f], and **Chun Li**[b,*]

[a]College of Pharmaceutical Sciences, Zhejiang University, Yuhangtang Road 388, Hangzhou 310058, People's Republic of China

[b]Department of Experimental Diagnostic Imaging, The University of Texas MD Anderson Cancer Center, Houston, Texas 77030

[c]Department of Veterinary Medicine and Surgery, The University of Texas MD Anderson Cancer Center, Houston, Texas 77030

[d]College of Pharmacy, Texas Southern University, 3100 Cleburne Street, Houston, Texas 77004

[e]Department of Biostatistics, The University of Texas MD Anderson Cancer Center, Houston, Texas 77030

[f]Department of Gynecologic Oncology and Cancer Biology, The University of Texas MD Anderson Cancer Center, Houston, Texas 77030

Abstract

Photothermal ablation (PTA) is an emerging technique that uses near-infrared (NIR) laser light-generated heat to destroy tumor cells. However, complete eradication of tumor cells with PTA is difficult because of uneven heat distribution in the treatment volume. We hypothesized that combining PTA with chemotherapy using a single multifunctional nanoconstruct that mediates simultaneous photothermal cell killing and drug release (photothermal-chemotherapy) would result in enhanced antitumor activity and reduced toxicity compared to chemotherapy alone. Doxorubicin (DOX) was loaded to hollow gold nanospheres (HAuNS) coated with polyethylene glycol (PEG). The pharmacokinetics and biodistribution of both DOX and HAuNS in the resulting nanoconstruct, DOX@PEG-HAuNS having different DOX:PEG:HAuNS ratios, were evaluated using dual isotope labeling techniques. The antitumor activity of DOX@PEG-HAuNS with DOX:PEG:HAuNS weight ratio of 1:3:1 (**NP3)** in combination with NIR laser was studied *in vitro* and *in vivo* using human MDA-MB-231 breast cancer and A2780 ovarian cancer cells. *In vitro*, **NP3** mediated PTA of both cancer cells and DOX release upon NIR laser treatment. *In vivo*, **NP3** showed slower clearance in blood and greater accumulation in tumors than free DOX. **NP3**-plus-NIR laser demonstrated greater antitumor activity than free DOX, **NP3**, or liposomal DOX. Moreover, **NP3** displayed significantly decreased systemic toxicity compared to free DOX or liposomal DOX. Enhanced antitumor effect with **NP3**-plus-laser can be attributed to both the cytotoxic effect of DOX released from **NP3** and the photothermal effect mediated by HAuNS. Slow release of DOX from **NP3** in normal tissues contributed to reduced systemic toxicity. Photothermal-chemotherapy exemplified by a single-agent nanoconstruct **NP3** is a promising approach to anticancer therapy.

[*]Corresponding Author: Chun Li, Department of Experimental Diagnostic Imaging-Unit 59, The University of Texas MD Anderson Cancer Center, Houston, Texas 77030; Tel: 713-792-5182; Fax: 713-794-5456; cli@mdanderson.org.

Keywords

Doxorubicin; Near-Infrared light; Triggered Release; Photothermal ablation therapy; Pharmacokinetics

1. Introduction

Thermal ablation is the use of heat to directly destroy tissue. Many different types of energy sources can be applied, including radiofrequency, high-intensity focused ultrasound, microwave, and laser [1–5]. Heating energy can be delivered by external or internal means, via interstitial, intraluminal, or intracavitary approaches [6]. Laser-induced photothermal ablation (PTA) has been used successfully for ablation of tumors throughout the body. For example, for the treatment of liver cancers, laser energy is delivered through optical fibers inserted into the tumor under imaging guidance [2, 3]. Laser-induced PTA has also been evaluated as an alternative to radical surgery for advanced and recurrent head and neck squamous cell carcinoma [7, 8]. However, because of absorption by normal tissues, the amount of energy deposited to the treatment volume is limited, which reduces the potency of the thermal killing effect.

To improve the efficacy and tumor selectivity of laser-induced PTA, light-absorbing materials (known as photothermal conducting agents) are introduced into tumor cells to mediate the photothermal effect. Various gold nanostructures, including silica-cored nanoshells, nanocages, and nanorods that absorb near-infrared (NIR) light (wavelength 700–850 nm), have been shown to be effective photothermal conducting agents [9–12]. Gold nanoparticles are known to be nontoxic and nonimmunogenic [13, 14], and absorption of NIR light is desirable because NIR light itself causes minimal thermal injury to normal tissues and optimally penetrates normal tissues [15, 16].

DOX is a widely used chemotherapeutic agent. Unfortunately, its clinical utility has been limited in many settings because of its high toxicity. Various delivery systems for DOX have been devised with the objectives of enhancing antitumor efficacy and reducing systemic toxicity [17, 18]. We hypothesized that combining PTA with DOX using a single nanoconstruct that mediates simultaneous photothermal effect and drug release (photothermal-chemotherapy) would result in enhanced antitumor activity and reduced toxicity compared to chemotherapy alone. Towards this end, we have loaded DOX onto hollow gold nanospheres (HAuNS) coated with polyethylene glycol (PEG), with remarkably high payload, and demonstrated rapid DOX release *in vitro* from the resulting complex DOX@PEG-HAuNS (NP) upon laser irradiation [19]. HAuNS are a novel class of gold nanoparticles that have plasmon absorption in the NIR region and that display a strong photothermal conducting property suitable for PTA. HAuNS' unique combination of small size (30–50 nm in diameter) and strong and tunable (520–950 nm) absorption band suggests that HAuNS are a promising photothermal conducting agent for a variety of biomedical applications, including imaging [20–23] and cancer therapy [24, 25]. A few studies have explored the potential utility of HAuNS as a novel delivery vehicle to shuttle biomolecules or to trigger drug release under NIR light irradiation [19, 26, 27].

In this work, we investigated the *in vivo* behaviors of different formulations of DOX@PEG-HAuNS, including pharmacokinetics, biodistribution, and antitumor activity. We found that DOX@PEG-HAuNS with DOX:PEG:HAuNS weight ratio of 1:3:1 (**NP3**) plus NIR laser illumination afforded significantly enhanced therapeutic efficacy and a marked reduction in toxicity compared to free DOX and liposomal DOX, which are both used clinically. Thus, **NP3** is a promising nanocarrier of DOX and a mediator of dual-modality cancer therapy.

2. Materials and Methods

Materials

DOX was obtained from Sigma-Aldrich (St. Louis, MO). Tritium-labeled DOX [^{3}H]DOX; 1.3 mCi/mg DOX) was obtained from Moravek Biochemicals Inc. (Brea, CA). $^{64}CuCl_2$ radionuclide was obtained from Washington University (St. Louis, MO). Liposomal doxorubicin was obtained from Ochem Incorporation (Des Plaines, IL). *O*-(2-aminoethyl)-*O*′-methylpolyethylene glycol with molecular weight of 5000 (MeO-PEG$_{5000}$-NH$_2$) was obtained from Fluka (Buchs, Switzerland). (3-(4,5-Dimethylthiazol-2-yl)-2,5-diphenyltetrazolium bromide (MTT) was from Sigma-Aldrich. Trisodium citrate dehydrate (>99%), cobalt chloride hexahydrate (99.99%), sodium borohydride (99%), and chloroauric acid trihydrate (ACS reagent grade) were purchased from Fisher Scientific (Pittsburgh, PA) and were used as received. Methylene chloride (ACS grade) was obtained from Baxter Healthcare Corp (Deerfield, IL).

Synthesis of HAuNS and DOX loading

HAuNS and DOX-loaded HAuNS were obtained according to our previously reported procedures [19]. For DOX loading, free DOX (16 mg) (Sigma-Aldrich, St. Louis, MO) in water (10 mL) was added into 30 mL of citrate solution of PEG-HAuNS (21.3 OD/mL), and the mixture was stirred at room temperature for 24 h. The resulting DOX-loaded PEG-HAuNS were purified by repeated centrifugation and washing steps. The diameter of the nanoparticles was determined by dynamic light scattering using a Zeta Plus particle analyzer (Brookhaven Instruments, UK). PEGylated HAuNS without DOX loading (**NP1**) and DOX-loaded HAuNS without PEG coating (**NP2**) were similarly prepared and used as controls.

Radiolabeling with ^{64}Cu and ^{3}H

For conjugation of radiometal chelator to HAuNS, 1,4,7,10-tetraazacyclododecane-*N,N*′,*N*″,*N*‴-tetraacetic acid thioctamide (DOTA-TA, 1.0 mg/mL; 20 μL) was mixed with 1.0 mL of aqueous solution of HAuNS (160 OD/mL) for 6 h at room temperature. PEGylated nanoparticles were obtained according to previously described procedures [19]. For radiolabeling with ^{64}Cu, aliquots of DOTA-coated PEG-HAuNS (160 OD/mL) in 0.1 M sodium acetate solution (pH 5.4) were mixed with an aqueous solution of^{64} $CuCl_2$ (10 mCi) for 1 h. The radiolabeled nanoparticles were then purified by centrifugation at 7155 *g* for 10 min and washed three times with PBS (pH7.4). The nanoparticles were then resuspended in sodium citrate solution (3.5 mM, pH 5.4). DOTA(^{64}Cu)-PEG-HAuNS were loaded with DOX to afford DOX@DOTA(^{64}Cu)-PEG-HAuNS according to procedures described in the previous section. The radiolabeling efficiency and the stability of labeled nanoparticles were analyzed using instant thin-layer chromatography. The paper strips were developed with PBS (pH 7.4) containing 4.0 mM ethylenediaminetetraacetic acid, and the radioactivity was quantified using a Bioscan IAR-2000 thin-layer chromatography imaging scanner (Washington, DC). Free $^{64}Cu^{2+}$ moved to the solvent front (Rf = 0.9–1.0), and the nanoparticles remained at the original spot (Rf = 0.0). The labeling efficiency was >95%. For dual labeling study, DOTA-PEG-HAuNS were labeled by ^{64}Cu and then mixed with a mixture of ^{3}H-DOX (200 μCi, 0.154 mg) and DOX (2.346 mg) to obtain ^{3}H-DOX@DOTA(^{64}Cu)-PEG-HAuNS (^{64}Cu-labeled, ^{3}H-DOX-loaded HAuNS).

Cellular uptake of free DOX and DOX-loaded HAuNS

MDA-MB-231 human breast carcinoma cells were purchased from the American Type Culture Collection (Manassas, VA) and were authenticated. A2780 human ovarian carcinoma cells were kindly provided by Dr. Stephen J. Williams (Fox Chase Cancer Center, Philadelphia, PA). The cells were maintained at 37oC in a humidified atmosphere

containing 5% CO_2 in Dulbecco's modified Eagle's medium and 10% fetal bovine serum (Life Technologies, Inc., Grand Island, NY). Cells were transferred and cultured onto 20-mm glass cover slips in a 24-well plate and allowed to grow for 2 days. The medium was then replaced with 1 mL of fresh culture medium containing free DOX or DOX-loaded HAuNS. After incubation for 2 h, cell nuclei were stained with DAPI. The cell monolayer on the cover slip was removed, repeatedly rinsed with PBS, and then mounted for microscopic examination. The cellular fluorescence and dark-field light scattering images were examined under a Zeiss Axio Observer Z1 fluorescence microscope (Carl Zeiss MicroImaging GmbH, Germany) equipped with a dark-field condenser.

In a separate experiment, MDA-MB-231 and A2780 cells (~1×10^6/dish) were cultured in 60 mm×15 mm dishes in culture medium without fetal bovine serum and phenol red. After the addition of free [^{3}H]-DOX or [^{3}H]-DOX loaded HAuNS (1.5 μCi /dish), culture dishes were sampled at predetermined time intervals. Cells were rinsed five times with PBS (pH 7.4). After removal of PBS, the cells were then scraped off the dish and suspended in PBS. Cell suspension was used for liquid scintillation counting and protein quantification. Protein was determined using the Bio-Rad assay kit (Richmond, CA).

Pharmacokinetics and biodistribution

All animal studies were carried out under Institutional Animal Care and Use Committee-approved protocols. For pharmacokinetic study, eight healthy female Swiss mice (22–25 g; Charles River Laboratories, Wilmington, MA) were each injected intravenously with a dose of ^{64}Cu-labeled HAuNS (20 μCi, 40 OD in 0.2 mL). At predetermined intervals (0 to ~24 h), blood samples (10 μL) were taken from the tail vein, and the radioactivity of each sample was measured with a gamma counter. The percentage of the injected dose per gram of blood (%ID/g) was calculated. The blood pharmacokinetic parameters for the radiotracer were analyzed using a noncompartmental model with WinNonlin 5.0.1 software (Pharsight, Palo Alto, CA). Mice were euthanized by CO_2 exposure at the end of the study (24 h after injection). Various tissues were removed, weighed, and radioactivity measured with a gamma counter. Uptake of the nanoparticles in various tissues was calculated as percentage of injected dose per gram of tissue (%ID/g).

Dual radiotracer technique for *in vivo* stability of DOX-loaded HAuNS

To investigate the *in vivo* distribution of DOX and HAuNS in the optimal formulation of DOX-loaded HAuNS (weight ratio of DOX:PEG:HAuNS = 1:3:1, **NP3**), nude mice (Harlan, Indianapolis, IN) bearing 6–8 mm subcutaneous A2780 tumors were injected intravenously with ^{64}Cu-labeled ^{3}H-**NP3** (5.0 mg equivalent DOX/kg; 25 OD in 0.2 mL; ^{3}H, 10 μCi/mouse; ^{64}Cu, 20 μCi/mouse;) or free ^{3}H-DOX (5.0 mg DOX/kg; ^{3}H, 10μCi/mouse). Mice were killed at 6, 24, and 48 h after injection. Various tissues including tumors were collected and split into two halves for radioactivity counting of ^{3}H-DOX and ^{64}Cu-PEG-HAuNS. For quantification of tissue contents of ^{3}H-DOX, 20 to ~50 mg of each tissue was weighed and solubilized in 1.0 mL of scintillation liquid, and the radioactivity measured by a liquid scintillation analyzer (Packard Bioscience Company, Meriden, CT). For quantification of tissue content of ^{64}Cu-labeled PEG-HAuNS, each tissue was wet-weighed, and radioactivity measured with a gamma counter. Uptake of DOX and PEG-HAuNS in various tissues was calculated as %ID/g.

MicroPET imaging

Mice bearing subcutaneous A2780 tumors were injected intravenously with ^{64}Cu-labeled **NP3** (8.0 mCi/kg, 25.6 OD). Mice were placed in the prone position, anesthetized with 0.5–2.0% isoflurane gas (Iso-Thesia, Rockville, NY) in oxygen. μPET images were acquired at

6 h and 24 h after injection using a Rodent R4 scanner (Concorde Microsystems, Inc. Knoxville, TN).

Photothermal ablation *in vitro*

For assessing PTA effect *in vitro*, A2780 cells seeded onto a 96-well plate were treated with **NP3** (3.2 OD/mL; 80 μg DOX/mL; 2 h) plus NIR laser, free DOX (80 μg DOX/mL; 2 h) plus NIR laser, or NIR laser alone. Laser treatment was achieved with NIR laser light centered at 808 nm at an output power of 32 W/cm^2 for 5 min (15PLUS laser, Diomed, Cambridge, UK). Twenty-four hours later, cells were washed and stained with calcein AM (Invitrogen, Carlsbad, CA) for visualization of live cells and with EthD-1 (Invitrogen) for visualization of dead cells. Cells were observed using a Zeiss Axio Observer Z1 fluorescence microscope.

Cytotoxicity

Cytotoxicity was measured using MTT assay according to the manufacturer's suggested procedures (Sigma-Aldrich). MDA-MB231 and A2780 cells were exposed to free DOX, **NP3** alone, or **NP3** plus laser for 48 h. The data are expressed as percentage of survival cells and are reported as the means of triplicate measurements.

Antitumor activity in *vivo*

MDA-MB-231 cells were inoculated into the mammary fat pads of female nude mice (5×10^6 cells/mouse). When the tumor volume reached ~200 mm^3, mice were divided into five groups consisting of 5–6 mice in each group. Mice in groups 1 to 4 were injected intravenously with 0.2 mL of saline (n = 5), free DOX (n = 5), liposomal DOX (DOXIL) (n = 6), and **NP3** (70 OD in 0.2 mL) (n = 5), respectively. Mice received two weekly injections at a dose of 15 mg equivalent DOX/kg per injection, except for mice in the free DOX group, which received a single dose because mice showed signs of a morbid state after the first dose. Mice in group 5 (n = 6) received the same **NP3** injection as in group 4, and were followed by NIR laser treatment (1.5 W/cm^2, for 5 min) 24 h after each drug injection. The tumor dimensions were measured twice weekly with a caliper, and the tumor volume was calculated according to the equation: Volume = (Tumor Length) × (Tumor Width)^2/2. Body weights were measured twice weekly. Experiment was terminated on day 24 days after initial treatment when tumors in the control group reached >1000 mm^3.

In a separate experiment, A2780 tumors were generated by subcutaneous injection of A2780 cells (8×10^6 cells/mouse). When the tumor volume reached ~500 mm^3 (~2 weeks after tumor inoculation), mice were divided into four groups consisting of six mice in each group. Mice in groups 1 to 4 were injected intravenously with single dose of saline, liposomal DOX (30 mg equivalent DOX/kg), **NP3** (140 OD in 0.2 mL, 30 mg equivalent DOX/kg), and **NP3** (140 OD in 0.2 mL, 30 mg equivalent DOX/kg), respectively. Mice in groups 4 were also irradiated with NIR laser (1.0 W/cm^2 for 5 min) at 24 h after drug injection. The tumor sizes and body weights were recorded as described in the preceding paragraph. Mice were killed on day 8 after the initiation of treatment when the body weight of the mice in the group treated with liposomal DOX decreased 20%.

Toxicity

For chronic toxicity study, a group of nude mice (n = 6) was injected with **NP3** at a single intravenous dose of 60 mg equivalent DOX/kg. The second group of nude mice (n = 5) was injected with free DOX at a single intravenous dose of 15 mg equivalent DOX/kg. In third group, mice (n = 6) received two injections of liposomal DOX at a dose of 15 mg equivalent DOX/kg per injection. In forth group, mice (n = 6) received two injections of saline as a

control group. Animals were killed on day 60 after drug injection by CO_2 euthanasia and organs collected and fixed in 10% neutral buffered formalin. Sections of heart, liver, spleen, kidney, and lung were paraffin-embedded, nominally cut at 5 μm thickness, stained with hematoxilin and eosin, and examined by a board certified veterinary pathologist.

Statistics

Tumor volume and body weight change were calculated as percent change from baseline (day 0) to day 8 (A2780 model) or day 24 (MDA-MB231 model). Percent change in tumor volume was calculated using the formula: [V(day 8 or day 24) – V(baseline)/V(baseline) x 100%. Summary statistics of percent change were provided in the form of mean, standard deviation (SD), and range by tumor cell line and treatment group. Due to the skewness in the data, percent changes were transformed using cubic root transformation prior to any statistical analysis. Analysis of variance (ANOVA) method was used to assess if there was any significant difference between all treatment groups with respect to tumor volume and body weight change at the time points specified above. Pairwise comparisons between treatment groups were only carried out if the overall significance was established first. The Tukey-Kramer adjustment was used to control overall type I error rate with multiple comparisons at each time point. Estimated group means as well as group differences and their corresponding 95% confidence intervals (CIs) were transformed back to raw scale for reporting. All tests were two-sided and p-values of 0.05 or less were considered statistically significant. Statistical analyses were carried out using SAS version 9 (SAS Institute, Cary, NC).

3. Results

DOX loading onto PEG-HAuNS

The physicochemical properties of citrate- coated HAuNS, PEG-HAuNS (**NP1**), and different formulations of DOX-loaded HAuNS are summarized in Table 1. For DOX@PEG-HAuNS (1:3:1, w:w:w) (**NP3**), DOX loading efficiency was ~95% and DOX content was 31.5% (w/w), measured by a previously reported method [19]. The extinction spectrum showed that the plasma resonance peak of PEG-HAuNS was tuned to the NIR region (~800 nm) and that DOX loading did not affect the characteristic extinction spectrum of PEG-HAuNS. The size of unPEGylated DOX@HAuNS (1:0:1, w:w:w) (**NP2**) was much larger than the size of other PEGylated HAuNS, indicating that without PEG coating, the nanoparticles are unstable. This is because DOX loading on HAuNS via electrostatic interaction decreased the stabilizing capability of citrate layer on the surface of HAuNS. Hydrophilic PEG chains chemically conjugated to HAuNS could overcome the de-stabilizing effect of DOX. The negatively charged **NP1** changed to positive after DOX loading (Table 1).

Cellular Uptake *in vitro*

Figure 1A shows dark-field and fluorescence images of A2780 cells incubated with free DOX and **NP3.** The nanoparticles were distributed into the cytoplasm of the cells. The fluorescence signal from DOX was mostly co-localized with the signal from HAuNS, indicating that DOX remained associated with HAuNS after **NP3** internalization. In contrast, free DOX was primarily localized to cell nuclei (Fig. 1A). Figure 1B compares kinetics of cellular uptake of free [^{3}H]DOX and [^{3}H]-**NP3** in MDA-MB-231 and A2780 cell lines. For both cell lines, at all time points (with the exception of A2780 cells at 6 h), uptake of [^{3}H]-**NP3** was significantly higher than uptake of free [^{3}H]DOX ($p<0.05$) (Fig. 1B). One possible explanation for the increased cellular uptake of [^{3}H]DOX in cells treated with [^{3}H]-**NP3** is the high payload of DOX in **NP3**. The positively charged **NP3** may also have contributed to

the enhanced interaction with tumor cells, which facilitates cellular uptake of **NP3** through phagocytic processes [28, 29].

Pharmacokinetics and biodistribution of ^{64}Cu-labeled HAuNS

Figure 2A shows the mean blood activity-time profile of 4 different formulations of DOX-loaded HAuNS. UnPEGylated **NP2** were cleared rapidly from the blood. Introducing PEG onto the surface of HAuNS resulted in significant increase in blood activity of the nanoparticles at all time points; HAuNS with higher PEG density (**NP1** and **NP3)** had higher blood activity than HAuNS nanoparticles with lower PEG density (**NP4**). The terminal biological half-life ($T_{1/2}$) of DOX-loaded HAuNS increased from 1.11 h for **NP2** to 7.06 h for **NP4**, about a sevenfold increase. The total area under the blood concentration versus time curve (AUC) also increased from 5.58 %ID/mL to 241 %ID/mL, which was about a 43-fold increase. With higher PEG density, $T_{1/2}$ further increased, to 8.82 h for **NP3**, and AUCincreased to 434 %ID/mL (Table 2).

Interestingly, DOX loading did not significantly affect the nanoparticles' behavior in blood when the ratio of PEG and HAuNS was kept constant. For example, the $T_{1/2}$ and AUC were 8.19 h and 434 %ID/mL, respectively, for **NP1** and were 8.82 h and 434 %ID/mL, respectively, for **NP3** (Fig. 2A and Table 2). Although the hydrodynamic size measured with light scattering differed by 1.9-fold between **NP1** (~44.7 nm) and **NP3** (~85.6 nm), these nanoparticles with different DOX loading had the same size for their HAuNS core. Previously, we have shown that the pharmacokinetic behavior of solid gold nanoparticles is influenced by the size of the hard Au core, which affected the density of PEG coating [30]. These earlier observations and the current data are consistent, and confirm that pharmacokinetic properties are primarily dictated by the density of PEG coating on the surface of HAuNS.

Biodistribution data for the various formulations of ^{64}Cu-labeled HAuNS at 24 h after injection are presented in Figure 2B. For HAuNS coated with PEG (**NP1**, **NP3**, and **NP4**), the distribution did not differ significantly by organ, and was high in blood. However, most **NP2** without PEG coating were taken up by the liver and the spleen 24 h after intravenous injection. On the basis of these results, **NP3** were used for further studies.

MicroPET images (Fig. 2C) indicated that ^{64}Cu-labeled **NP3** showed significant blood pool activity and high uptake in the liver and spleen over the entire study period, which was consistent with the biodistribution data. By 24 h after injection, the accumulation of **NP3** in the tumor was readily visualized. The tumor localization of the nanoparticles could be attributed to the enhanced permeability and retention effect of long-circulating nanoparticles.

In vivo stability of NP3 assessed by dual radiotracer technique

At 6 h after injection of **NP3** containing [^{3}H]DOX and [^{64}Cu]HAuNS, DOX and HAuNS had similar biodistribution patterns in most tissues (Fig. 3A), which suggested that there was negligible release of DOX from HAuNS *in vivo* during this period. However, DOX gradually detached from **NP3** later in the time course (>24 h). HAuNS from **NP3** were cleared slowly from most tissues and organs (with the exception of blood, from which HAuNS were cleared rapidly) between 6 h and 24 h after injection as measured with ^{64}Cu activity. In contrast, DOX from **NP3** was cleared significantly more rapidly than HAuNS did from most tissues, with the exception of spleen (Fig. 3A).

The biodistribution of free [^{3}H]DOX injected at the same equivalent dose was also studied and the data in comparison with [^{3}H]-**NP3** are presented in Figure 3B. Free DOX clearly

showed significantly faster blood clearance than DOX from [^{3}H]-**NP3** did. Only 0.168 %ID/g was present in the blood at 6 h after [^{3}H]DOX injection, whereas for [^{3}H]-**NP1**, 8.61 %ID/g was present in the blood at 6 h. **NP3** increased the accumulation of DOX in tumors as compared to free DOX; tumor uptake of [^{3}H]DOX increased from 1.08 %ID/g for free DOX to 3.70 %ID/g for **NP3** with about 3.5-fold increase at 6 h after injection (p=0.015) (Fig. 3B). By 48 h after injection, free [^{3}H]DOX showed less tissue uptake than [^{3}H]-**NP3** in all organs analyzed. Tumor uptake of [^{3}H]DOX increased from 0.46 %ID/g for DOX to 2.08 %ID/g for **NP3** with about 4.5-fold increase at 48 h after injection (p=0.012) (Supplementary Fig. S1).

Photothermal ablation *in vitro*

After NIR laser irradiation at an output power of 32 W/cm^2 for 5 min, there was a clear boundary between the area irradiated with laser and the area not exposed to laser in cells treated with **NP3** (Fig. 4A). In the area with NIR laser irradiation, most cells were stained red, while in the area without NIR laser irradiation, most cells were stained green with calcein AM, which indicated selective cell ablation for cells exposed to NIR laser. In comparison, there was no differential cell killing between laser-irradiated and non-irradiated zones either in cells treated with free DOX or in untreated control cells.

Cytotoxicity *in vitro*

NP3 showed a chemotherapeutic effect *in vitro* against MDA-MB-231 and A2780 cells in a dose-dependent manner; the concentrations causing death of 50% of the cells (IC_{50}s) were 27.93 and 0.834 μM, respectively (Fig. 4B). Compared with **NP3**, free DOX exhibited higher toxicity, with IC_{50}s of 2.83 and 0.094 μM, respectively against MDA-MB-231 and A2780 cells. The lower cell killing potency with **NP3** could be attributed to relatively stable complexes formed between DOX and PEG-HAuNS and delayed DOX release inside cells. Tumor cell killing potency of **NP3** was enhanced when **NP3** were combined with NIR irradiation; the IC_{50}s of **NP3** plus NIR laser were 2.52 and 0.031 μM respectively against MDA-MB-231 andA2780 cells.

Antitumor activity *in vivo*

Figure 5 shows the MDA-MB-231 tumor-growth curves after two weekly intravenous injections of saline, liposomal DOX (15 mg equivalent DOX/kg/injection), **NP3** (15 mg equivalent DOX/kg/injection), and **NP3** (15 mg equivalent DOX/kg/injection) followed by NIR laser treatment (1.5 W/cm^2 for 5 min) 24 h after drug injection. Free DOX (15 mg/kg) was only given once because of significant body weight loss after the first dose. Supplementary Table S1 summarizes percent change in tumor volume on day 24 after the initiation of treatment when all tumors in the saline control had reached ~1000 cm^3. There was no significant difference in tumor size between groups treated with **NP3**, free DOX, and liposomal DOX. However, **NP3**-plus-NIR laser reduced tumor volume significantly more than all other treatments by day 24 (Supplementary Table S1). In fact, the tumors in three of the six mice treated with **NP3**-plus-NIR laser were reduced to scar tissue by 20 days after the initiation of treatment. The tumors in this group of mice became whitish immediately after treatment, suggesting disruption of blood perfusion (Fig. 5B).

Similar results were obtained when **NP3** were tested using another tumor model, A2780 ovarian carcinoma (Supplementary Table S1 and Fig. S2). In this experiment, the **NP3** dose was increased 2-fold to 30 mg equivalent DOX/kg with a single injection. Antitumor activity against subcutaneously inoculated A2780 tumors was significantly higher with combined **NP3**-plus-NIR laser than with saline (p<0.0001), **NP3** alone (showing antitumor effect of DOX released from HAuNS; p<0.0001,), or liposomal DOX (p < 0.0001).

Toxicity

With the two weekly dosing schedule at a dose of 15 mg equivalent DOX per injection, **NP3**-plus-NIR laser was moderately toxic compared to **NP3** alone or saline. However, the treatment did not show significant difference compared with any other treatment group with regard to body weight change on day 24 (Supplementary Table S1 and Fig. 5C). With the single injection dosing schedule at a dose of 30 mg equivalent DOX, the combination of **NP3**-plus-NIR laser treatment was significantly less toxic than liposomal DOX (Supplementary Table S1 and Fig. S2). **NP3**-plus-NIR laser was more toxic than saline and **NP3** alone. Whereas groups of mice treated with saline and **NP3** gained an average of 17.7% weight and 13.2%, respectively, mice treated with **NP3**-plus-NIR laser only gained 2.3% by body weight on day 8 after treatment.

The chronic toxicity was evaluated on day 60 after intravenous injection. H&E stained sections from the heart, liver, spleen, kidney, and heart were examined. Histopathology data indicates that **NP3** after a single dose at 60 mg equivalent DOX/kg had no cardiotoxicity compared to liposomal DOX (two doses at a total dose of 30 mg DOX/kg) and free DOX (single dose of 15 mg/kg) (Fig. 6). The free DOX group (a single dose of 15 mg/kg) had the most morbidity; 3 of 5 animals were found dead and postmortem autolysis precluded histopathologic analysis. In the heart, 100% of both liposomal DOX and free DOX animals had a vacuolar cardiomyopathy. However, for the **NP3** group, the histopathologic features in the heart were similar to those observed in the saline-treated control group and no abnormal features were observed (Fig. 6).

A treatment-related increase in pigment occurred in all treated groups, but was more prevalent in the **NP3** than the DOX group. The pigment was most prevalent in the liver in primarily the Kupffer cells and occasionally in the hepatocytes, and was associated with minimal to slight inflammation. Pigment was also present in macrophages of the spleen and in myocardiocytes of the heart. The kidneys did not have pigment deposition, but an increase in incidence and severity of chronic glomerulonephropathy in groups treated with the free DOX and liposomal DOX. No abnormality was noted in the group treated with **NP3** (Fig. 6). The pigment stained positive using a Schmorl's stain in the heart, liver, and spleen suggesting it may be lipofuscin (Supplementary Table S2). Additional studies are needed to further evaluate the nature of the pigment and hepatic function in mice treated with **NP3**.

Discussion

The findings from our present study indicate that photothermal-chemotherapy, the combination of PTA and chemotherapy mediated by injection of **NP3** followed by NIR laser irradiation, did in fact result in enhanced antitumor activity compared to free DOX, liposomal DOX and **NP3** alone. Our data also indicate that **NP3** exhibited reduced systemic toxicity compared to free DOX and liposomal DOX.

Our finding that ^{3}H-DOX and ^{64}Cu-PEG-HAuNS had a similar biodistribution pattern in most tissues during the first 6 h after intravenous injection of dual-labeled **NP3** suggest that there is negligible release of DOX from PEG-HAuNS during this period (Fig. 3A). A similar investigation by Liu et al [31] of ^{3}H-paclitaxel-loaded carbon nanotubes showed stable attachment of paclitaxel to carbon nanotubes for just 30 min *in vivo*. Therefore, DOX and PEG-HAuNS appears to have tighter association *in vivo* than paclitaxel and carbon nanotubes. A more stable association between a drug and its carrier in the blood circulation should cause less systemic toxicity and fewer side effects but may also decrease antitumor efficacy. However, when PEG-HAuNS are used as the carrier, as in our current study, NIR laser irradiation triggers local DOX release at the tumor site because of the photothermal conducting effect of HAuNS [19]. Moreover, DOX accumulation cancer cells was higher

with [^{3}H]-**NP3** than with free [^{3}H]DOX (Fig. 1B). Thus, it is anticipated that treatment with **NP3** and NIR laser should result in increased antitumor activity with reduced toxicity.

Our finding of significantly enhanced cytotoxicity for **NP3** plus NIR laser versus **NP3** alone in two cancer cell lines (Fig. 4B) can be attributed to three effects: 1) the PTA effect, by which laser light is converted by HAuNS to thermal energy, 2) increased intracellular concentration of free DOX due to NIR-triggered DOX release [19], and 3) a synergistic interaction between the photothermal effect and DOX's cytotoxic effect. It was previously reported that at temperatures above 40°C, cellular injury or death occurs because of protein denaturation, and that at higher temperatures (i.e., 85–90°C), DNA and RNA denature or unfold [32]. The exposure of cancer cells preincubated with **NP3** to NIR laser irradiation could cause a direct cell-killing effect owning to heat-induced protein denaturation and/or DNA or RNA injury. Second, **NP3** nanoparticles were efficiently taken up by cancer cells (Fig. 1). Thus, the increased DOX concentration in the tumor cells due to NIR-triggered DOX release could lead to increased cytotoxicity observed with **NP3**-plus-NIR laser versus **NP3** alone [19]. Lastly, the synergistic cytotoxic effects between chemotherapeutic agent and hyperthermia have been well documented in previous other work [33–36].

Although up to 60% by weight of DOX could be loaded to HAuNS [19], antitumor activity and toxicity studies were performed only with **NP3** with 31.5% DOX loading. The doses of free DOX and **NP3** were chosen based on our preliminary dose survey study. Our measurements of the body weight of mice with MDA-MB-231 and A2780 tumors exposed to various treatments suggested that **NP3** were moderately toxic but less toxic than free DOX and liposomal DOX. Mice treated with a single 15 mg/kg dose of free DOX lost ~10% of their body weight during the first 5 days after drug administration and became morbid and weak. These results suggested that the maximum tolerated dose (MTD) of free DOX was less than 15 mg equivalent DOX/kg, which agrees with previous reports [37]. Liposomal DOX at a twice weekly dose of 15 mg DOX/kg per injection caused a maximal 10% decrease in body weight (Fig. 5C). In addition, liposomal DOX caused a 20% decrease in body weight after a single dose of 30 mg DOX/kg (Supplementary Fig. S2). In contrast, the body weight of mice in the **NP3** treatment group after 2 doses at 15 mg/kg per dose kept increasing during the whole experimental period. Even at a single dose of 60 mg equivalent DOX/kg, there were no observable signs of toxicity or loss of body weight over a period of 2 months (data not shown), which suggested that the single dose MTD of **NP3** was equal or greater than 60 mg equivalent DOX/kg, at least four times the MTD for free DOX. For mice in the **NP3**-plus-NIR laser treatment group, the body weight dropped initially (suggesting that some free DOX was released and re-entered the system) but recovered quickly and then gradually increased during the remainder of the experimental period (Fig. 5C and Supplementary Fig. S2).

It is well known that DOX can cause cardiac damage [38], and that liposomal DOX lessens the heart damage from DOX because it has lower blood concentration of free DOX [39–41]. In a 60-day study period, **NP3** caused less toxic effect to the heart than free DOX and liposomal DOX (Fig. 6). In the same chronic toxicity study, increased pigment was noted primarily in the macrophages of the liver and the spleen. This may be attributed to increased uptake and retention of the nanoparticles in these organs. Additional studies are needed to further evaluate the nature of the pigment and hepatic function in mice treated with **NP3**.

Conclusions

Taken together, our data indicate that treatment of mice with **NP3** followed by NIR laser irradiation had significantly greater antitumor activity than treatment with **NP3** alone, free DOX and liposomal DOX. It is anticipated that if lower equivalent DOX doses were used,

the therapeutic gain achievable with **NP3**-plus-NIR laser as compared to the same equivalent dose of free DOX, **NP3**, or liposomal DOX would have been even greater. Combining **NP3** and laser treatment resulted in reduced toxicity compared to free DOX and liposomal DOX. Enhanced antitumor effect with **NP3**-plus-laser can be attributed to both the cytotoxic effect of DOX released from **NP3** and the photothermal effect mediated by HAuNS under NIR laser exposure. In normal tissues, DOX was slowly released from **NP3**, resulting in a decreased systemic toxicity. The photothermal-chemotherapy strategy mediated through a single nanoconstruct exemplified by **NP3** represents a promising approach to effective anticancer therapy.

Supplementary Material

Refer to Web version on PubMed Central for supplementary material.

Acknowledgments

The authors thank Stephanie Deming for editing the manuscript and Dr. Sherry Klumpp for histologic evaluation. We also thank Mr. Kenneth Dunner for assistance with the TEM facility. This work was supported in part by National Cancer Institute grants R01 CA119387 and U54 CA151668, the John S. Dunn Foundation, a seed grant through the Alliance for NanoHealth in Houston by the U.S. Department of Army Telemedicine and Advanced Technology Research Center (W81XWH-07-02-0101), and the National Nature Science Foundation of China (grant 81008411 to JY). We also acknowledge the NCI Cancer Center Support Grant CA016672, which supports MD Anderson's Small Animal Imaging Facility and TEM Core Facility.

References

1. Curley SA, Izzo F, Delrio P, Ellis LM, Granchi J, Vallone P, Fiore F, Pignata S, Daniele B, Cremona F. Radiofrequency ablation of unresectable primary and metastatic hepatic malignancies: results in 123 patients. Ann Surg. 1999; 230:1–8. [PubMed: 10400029]
2. Fiedler VU, Schwarzmaier HJ, Eickmeyer F, Muller FP, Schoepp C, Verreet PR. Laser-induced interstitial thermotherapy of liver metastases in an interventional 0.5 Tesla MRI system: technique and first clinical experiences. J Magn Reson Imaging. 2001; 13:729–737. [PubMed: 11329194]
3. Vogl TJ, Straub R, Eichler K, Sollner O, Mack MG. Colorectal carcinoma metastases in liver: laser-induced interstitial thermotherapy--local tumor control rate and survival data. Radiology. 2004; 230:450–458. [PubMed: 14688400]
4. Seki T, Wakabayashi M, Nakagawa T, Itho T, Shiro T, Kunieda K, Sato M, Uchiyama S, Inoue K. Ultrasonically guided percutaneous microwave coagulation therapy for small hepatocellular carcinoma. Cancer. 1994; 74:817–825. [PubMed: 8039109]
5. Liapi E, Geschwind JFH. Transcatheter and ablative therapeutic approaches for solid malignancies. J Clin Oncol. 2007; 25:978–986. [PubMed: 17350947]
6. Diederich CJ. Thermal ablation and high-temperature thermal therapy: overview of technology and clinical implementation. Int J Hyperthermia. 2005; 21:745–753. [PubMed: 16338857]
7. Paiva MB, Blackwell KE, Saxton RE, Bublik M, Liu CD, Paolini AAPP, Calcaterra TC, Castro DJ. Nd : YAG laser therapy for palliation of recurrent squamous cell carcinomas in the oral cavity. Lasers Surg Med. 2002; 31:64–69. [PubMed: 12124717]
8. Paiva MB, Blackwell KE, Saxton RE, Calcaterra TC, Ward PH, Soudant J, Castro DJ. Palliative laser therapy for recurrent head and neck cancer: A phase II clinical study. Laryngoscope. 1998; 108:1277–1283. [PubMed: 9738741]
9. Loo C, Lin A, Hirsch L, Lee MH, Barton J, Halas N, West J, Drezek R. Nanoshell-enabled photonics-based imaging and therapy of cancer. Technol Cancer Res Treat. 2004; 3:33–40. [PubMed: 14750891]
10. El-Sayed IH, Huang X, El-Sayed MA. Selective laser photo-thermal therapy of epithelial carcinoma using anti-EGFR antibody conjugated gold nanoparticles. Cancer Lett. 2006; 239:129–135. [PubMed: 16198049]

11. Skrabalak SE, Au L, Lu X, Li X, Xia Y. Gold nanocages for cancer detection and treatment. Nanomed. 2007; 2:657–668.
12. Dreaden EC, Mackey MA, Huang X, Kang B, El-Sayed MA. Beating cancer in multiple ways using nanogold. Chem Soc Rev. 2011
13. Connor EE, Mwamuka J, Gole A, Murphy CJ, Wyatt MD. Gold nanoparticles are taken up by human cells but do not cause acute cytotoxicity. Small. 2005; 1:325–327. [PubMed: 17193451]
14. Male KB, Lachance B, Hrapovic S, Sunahara G, Luong JH. Assessment of cytotoxicity of quantum dots and gold nanoparticles using cell-based impedance spectroscopy. Anal Chem. 2008; 80:5487–5493. [PubMed: 18553941]
15. Weissleder R. A clearer vision for in vivo imaging. Nat Biotechnol. 2001; 19:316–317. [PubMed: 11283581]
16. Wang W, Ke S, Wu QP, Charnsangavej C, Gurfinkel M, Gelovani JG, Abbruzzese JL, Sevick-Muraca EM, Li C. Near-infrared optical imaging of integrin avb3 in human tumor xenografts. Mol Imaging. 2004; 3:343–351. [PubMed: 15802051]
17. Elsadek B, Kratz F. Impact of albumin on drug delivery - New applications on the horizon. J Control Release. 2011
18. Geers B, Lentacker I, Cool S, Demeester J, De Smedt SC, Sanders NN. Ultrasound responsive doxorubicin-loaded microbubbles; towards an easy applicable drug delivery platform. J Control Release. 2010; 148:e59–60.
19. You J, Zhang G, Li C. Exceptionally high payload of doxorubicin in hollow gold nanospheres for near-infrared light-triggered drug release. ACS Nano. 2010; 4:1033–1041. [PubMed: 20121065]
20. Wu CF, Liang XP, Jiang HB. Metal nanoshells as a contrast agent in near-infrared diffuse optical tomography. Opt Commun. 2005; 253:214–221.
21. Lee S, Chon H, Lee M, Choo J, Shin SY, Lee YH, Rhyu IJ, Son SW, Oh CH. Surface-enhanced Raman scattering imaging of HER2 cancer markers overexpressed in single MCF7 cells using antibody conjugated hollow gold nanospheres. Biosen Bioelectron. 2009; 24:2260–2263.
22. Schwartzberg AM, Oshiro TY, Zhang JZ, Huser T, Talley CE. Improving nanoprobes using surface-enhanced Raman scattering from 30-nm hollow gold particles. Anal Chem. 2006; 78:4732–4736. [PubMed: 16808490]
23. Lu W, Huang Q, Ku G, Wen X, Zhou M, Guzatov D, Brecht P, Su R, Oraevsky A, Wang LV, Li C. Photoacoustic imaging of living mouse brain vasculature using hollow gold nanospheres. Biomaterials. 2010; 31:2617–2626. [PubMed: 20036000]
24. Melancon MP, Lu W, Yang Z, Zhang R, Cheng Z, Elliot AM, Stafford J, Olson T, Zhang JZ, Li C. In vitro and in vivo targeting of hollow gold nanoshells directed at epidermal growth factor receptor for photothermal ablation therapy. Mol Cancer Ther. 2008; 7:1730–1739. [PubMed: 18566244]
25. Lu W, Xiong C, Zhang G, Huang Q, Zhang R, Zhang JZ, Li C. Targeted photothermal ablation of murine melanomas with melanocyte-stimulating hormone analog-conjugated hollow gold nanospheres. Clin Cancer Res. 2009; 15:876–886. [PubMed: 19188158]
26. Lu W, Zhang G, Zhang R, Flores LG II, Huang Q, Gelovani JG, Li C. Tumor site-specific silencing of NF-kappaB p65 by targeted hollow gold nanosphere-mediated photothermal transfection. Cancer Res. 2010; 70:3177–3188. [PubMed: 20388791]
27. Wu G, Mikhailovsky A, Khant HA, Fu C, Chiu W, Zasadzinski JA. Remotely triggered liposome release by near-infrared light absorption via hollow gold nanoshells. J Am Chem Soc. 2008; 130:8175–8177. [PubMed: 18543914]
28. Wong HL, Bendayan R, Rauth AM, Xue HY, Babakhanian K, Wu XY. A mechanistic study of enhanced doxorubicin uptake and retention in multidrug resistant breast cancer cells using a polymer-lipid hybrid nanoparticle system. J Pharmacol Exp Ther. 2006; 317:1372–1381. [PubMed: 16547167]
29. Yan Y, Johnston AP, Dodds SJ, Kamphuis MM, Ferguson C, Parton RG, Nice EC, Heath JK, Caruso F. Uptake and intracellular fate of disulfide-bonded polymer hydrogel capsules for Doxorubicin delivery to colorectal cancer cells. ACS Nano. 2010; 4:2928–2936. [PubMed: 20420377]

30. Zhang G, Yang Z, Lu W, Zhang R, Huang Q, Tian M, Li L, Liang D, Li C. Influence of anchoring ligands and particle size on the colloidal stability and in vivo biodistribution of polyethylene glycol-coated gold nanoparticles in tumor-xenografted mice. Biomaterials. 2009; 30:1928–1936. [PubMed: 19131103]

31. Liu Z, Chen K, Davis C, Sherlock S, Cao Q, Chen X, Dai H. Drug delivery with carbon nanotubes for in vivo cancer treatment. Cancer Res. 2008; 68:6652–6660. [PubMed: 18701489]

32. He XM, Wolkers WF, Crowe JH, Swanlund DJ, Bischof JC. In situ thermal denaturation of proteins in dunning AT-1 prostate cancer cells: Implication for hyperthermic cell injury. Ann Biomed Eng. 2004; 32:1384–1398. [PubMed: 15535056]

33. Hahn GM, Shiu EC. Effect of pH and elevated temperatures on the cytotoxicity of some chemotherapeutic agents on Chinese hamster cells in vitro. Cancer Res. 1983; 43:5789–5791. [PubMed: 6196107]

34. Yoo J, Lee YJ. Effect of hyperthermia and chemotherapeutic agents on TRAIL-induced cell death in human colon cancer cells. J Cell Biochem. 2008; 103:98–109. [PubMed: 17520700]

35. Adachi S, Kokura S, Okayama T, Ishikawa T, Takagi T, Handa O, Naito Y, Yoshikawa T. Effect of hyperthermia combined with gemcitabine on apoptotic cell death in cultured human pancreatic cancer cell lines. Int J Hyperthermia. 2009; 25:210–219. [PubMed: 19437237]

36. Ko SH, Ueno T, Yoshimoto Y, Yoo JS, Abdel-Wahab OI, Abdel-Wahab Z, Chu E, Pruitt SK, Friedman HS, Dewhirst MW, Tyler DS. Optimizing a novel regional chemotherapeutic agent against melanoma: hyperthermia-induced enhancement of temozolomide cytotoxicity. Clin Cancer Res. 2006; 12:289–297. [PubMed: 16397054]

37. Barraud L, Merle P, Soma E, Lefrancois L, Guerret S, Chevallier M, Dubernet C, Couvreur P, Trepo C, Vitvitski L. Increase of doxorubicin sensitivity by doxorubicin-loading into nanoparticles for hepatocellular carcinoma cells in vitro and in vivo. J Hepatol. 2005; 42:736–743. [PubMed: 15826724]

38. Weiss RB. The anthracyclines - will we ever find a better doxorubicin. Sem Oncol. 1992; 19:670–686.

39. Batist G, Harris L, Azarnia N, Lee LW, Daza-Ramirez P. Improved anti-tumor response rate with decreased cardiotoxicity of non-pegylated liposomal doxorubicin compared with conventional doxorubicin in first-line treatment of metastatic breast cancer in patients who had received prior adjuvant doxorubicin: results of a retrospective analysis. Anti-Cancer Drugs. 2006; 17:587–595. [PubMed: 16702817]

40. Leonard RCF, Williams S, Tulpule A, Levine AM, Oliveros S. Improving the therapeutic index of anthracycline chemotherapy: Focus on liposomal doxorubicin (Myocet (TM)). Breast. 2009; 18:218–224. [PubMed: 19656681]

41. Batist G. Cardiac safety of liposomal anthracyclines. Cardiovasc Toxicol. 2007; 7:72–74. [PubMed: 17652807]

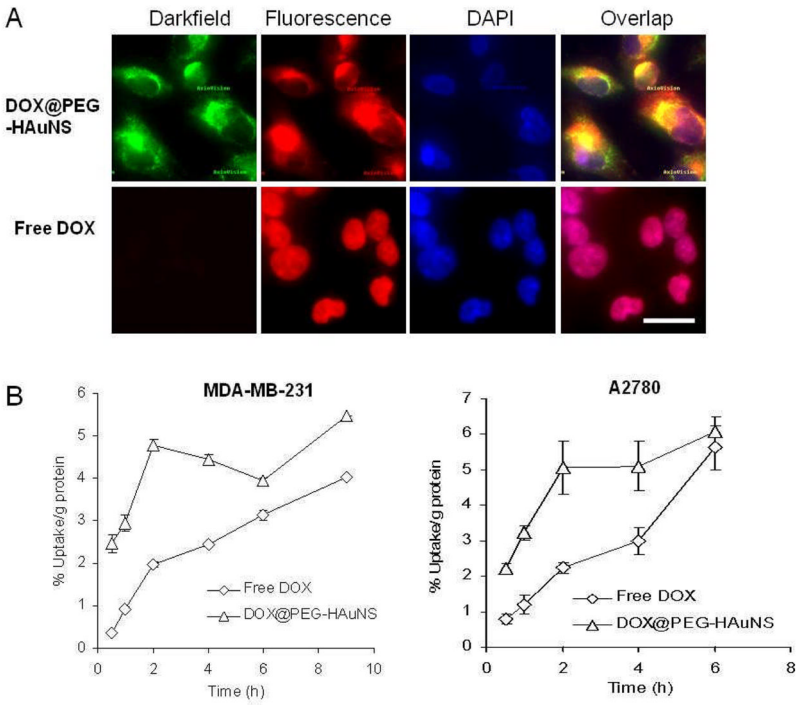

Fig. 1.

(A). Cellular uptake of free DOX (~80 μg/mL) and **NP3** (~80 μg equivalent DOX/mL, 0.32 OD/mL) in A2780 cells after 2-h incubation. The reflectance of PEG-HAuNS was visualized using a dark-field condenser. Cell nuclei were counterstained with DAPI (blue). Bar, 20 μm. **(B).** Kinetics of cellular uptake of free [^{3}H]DOX and [^{3}H]-**NP3** in MDA-MB-231 and A2780 cells. An equivalent DOX dose of 9.35 μg/mL (0.75 μCi/mL) was used for both drugs.

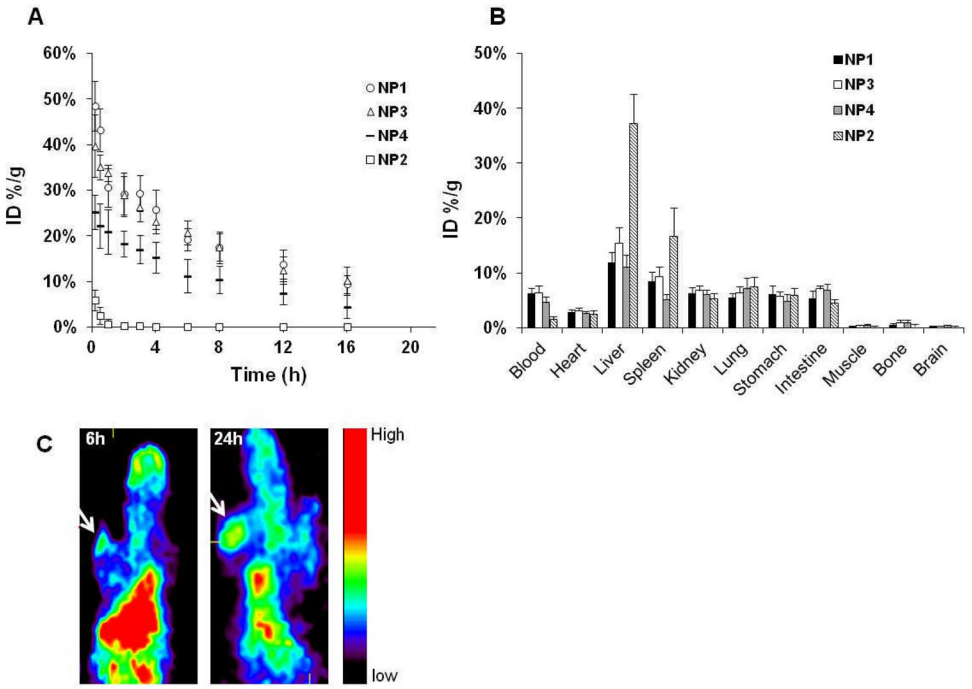

Fig. 2.

(A). Activity-time profiles of different HAuNS formulations in blood. **(B).** Biodistribution of different HAuNS formulations at 24 h in Swiss mice. The data are expressed as percentage of the injected dose per gram of tissue (%ID/g) and are presented as mean ± standard deviation (n = 8). In (A) and (B), the numbers in parentheses indicate the weight ratios of DOX:PEG:HAuNS in each formulation. **(C).** μPET images of mice bearing A2780 tumors after intravenous injection of ^{64}Cu-labeled **NP3**. Arrows, tumor.

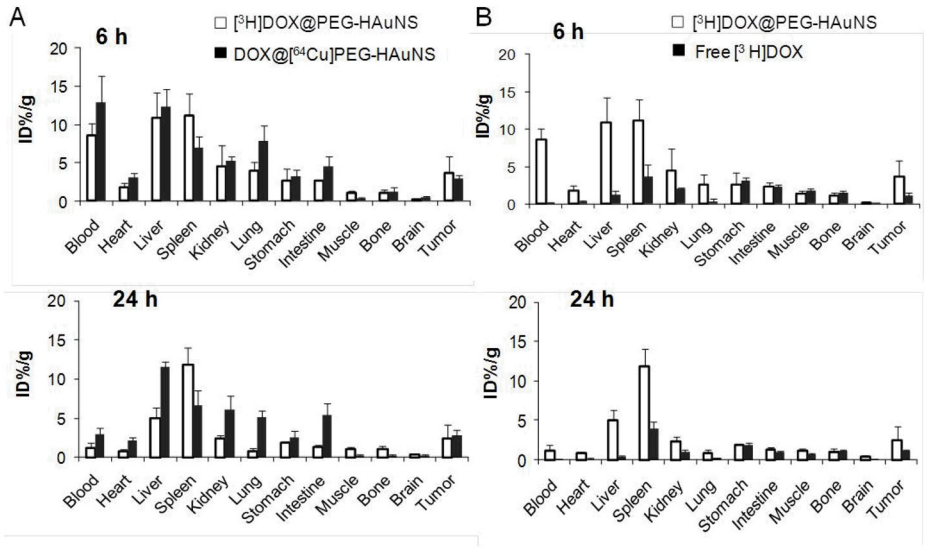

Fig. 3.

(A). Biodistribution of **NP3** labeled with both ^{3}H (for DOX) and ^{64}Cu (for HAuNS) at 6 h and 24 h after injection in mice bearing subcutaneous A2780 ovarian tumors. **(B).** Biodistribution of free [^{3}H]DOX and [^{3}H]-**NP3** at 6 and 24 h after injection. The data are expressed as percentage of the injected dose per gram of tissue (%ID/g) and are presented as mean ± standard deviation (n = 6).

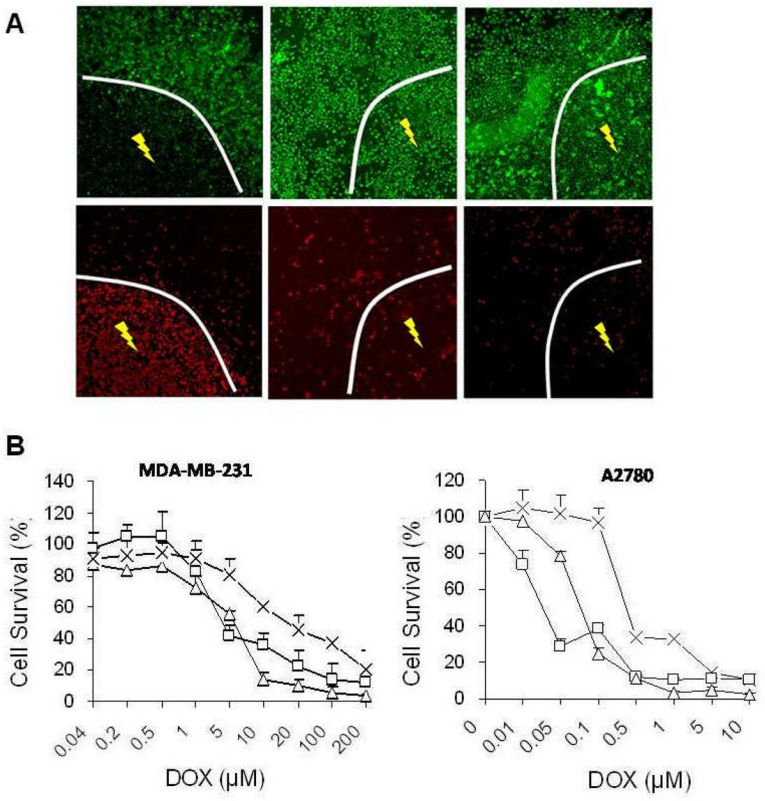

Fig. 4.

(A). PTA in A2780 cells with **NP3**. NIR laser was delivered at an output power of 32 W/cm^2 for 5 min. Cells were stained with calcein AM (green) and EthD-1 (red) for visualization of live and dead cells, respectively. **(B).** Cell viability as a function of equivalent DOX concentration. Cells were treated with free DOX (□),**NP3** (×), or **NP3**-plus-NIR laser (▽). The viability of cells was determined using the MTT assay. Data are expressed as mean ± standard deviation of triplicate measurements.

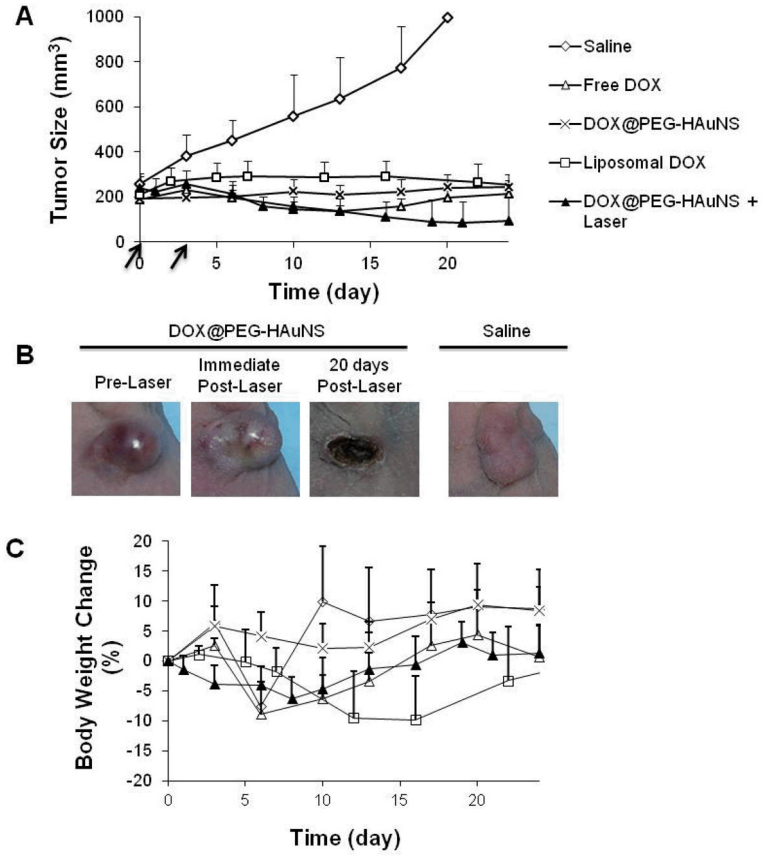

Fig. 5.

Antitumor activity *in vivo* against MDA-MB-231 tumor. **(A).** MDA-MB-231 tumor growth in mice treated with saline, free DOX, liposomal DOX, **NP3**, and **NP3**-plus-NIR laser irradiation. Arrows indicate dates of injection of each dose of 15 mg equivalent DOX/kg. In the free DOX group, the mice were injected only once on day 0. In the **NP3**-plus-laser group, tumor irradiation (1.5 W/cm^2 for 5 min) was commenced 24 h after nanoparticles injection. **(B).** Photographs of MDA-MB-231 tumors after treatment with **NP3**-plus-laser. **(C).** Percentage of mean body weight change. For (A) and (C), the data are presented as mean ± standard deviation (n = 5–7).

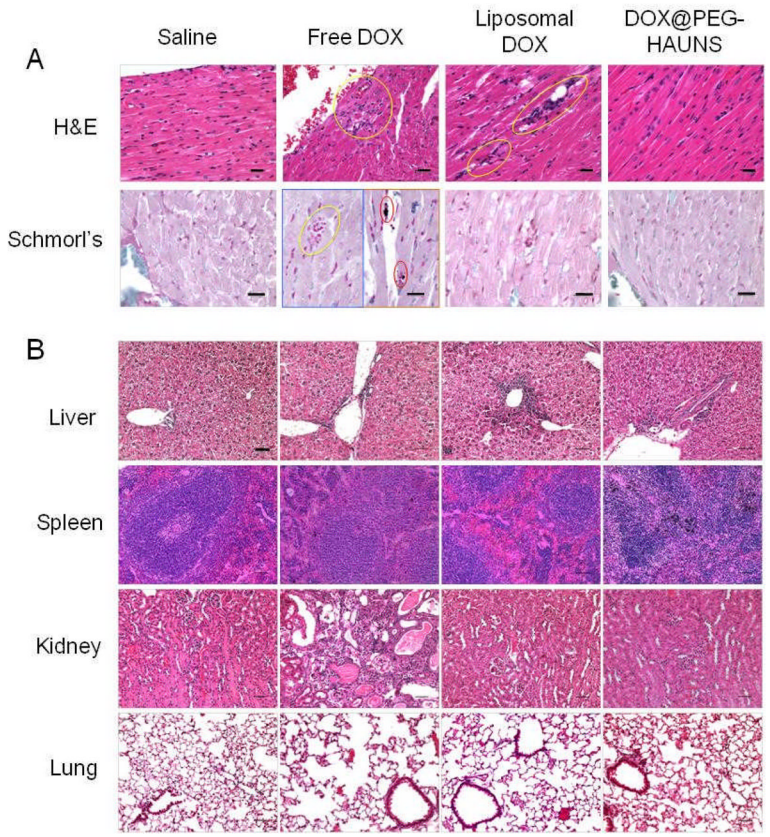

Fig. 6.

Histologic evaluation of tissues from mice treated with saline, free DOX (single dose at 15 mg/kg), liposomal DOX (2 doses at 15 mg DOX/kg each), and **NP3** (single dose at 60 mg DOX/kg). **(A).** Heart was sliced with 5-μm thickness for hematoxylin & eosin (H&E) and Schmorl's staining. The yellow circles indicate areas of necrosis or inflammation of the heart. Schmorl's staining confirmed some pigment (black dots in red circles) in the free DOX group and vacuoles in the liposomal DOX group. Bar, 20 μm. **(B).** Microphotographs of liver, spleen, kidney, and lung from mice in various treatment groups stained with H&E.

Table 1

Physicochemical properties of HAuNS, PEG-HAuNS, and 3 different formulations of DOX@PEG-HAuNS

	Citrate-HAuNS	PEG-HAuNS (0:3:1) (NP1)	DOX@PEG-HAuNS		
Ratio (W:W:W)[a]			**1:0:1 (NP2)**	**1:3:1 (NP3)**	**3:1:1 (NP4)**
Size (nm)	36.8±0.7	44.7±1.1	523.7±64.4	85.6±2.8	128.1±21.1
Zeta potential (mA)	−22.3±1.5	−16.7±2.8	7.2±1.2	14.1±2.7	17.6±1.6

[a]W:W:W, weight ratio of DOX:PEG:HAuNS.

J Control Release. Author manuscript; available in PMC 2013 January 10.

Table 2

Comparative pharmacokinetic parameters for various HAuNS formulations in mice after intravenous injection

Parameter[a]	DOX:PEG:HAuNS (W:W:W)[b]			
	0:3:1 (NP1)	**1:0:1 (NP2)**	**1:3:1 (NP3)**	**3:1:1 (NP4)**
$T_{1/2}$ (hr)	8.19 (1.4)	1.11 (1.2)	8.82 (1.3)	7.06 (3.2)
AUC (%ID/mL Blood)	434 (61)	5.58 (1.3)	434 (88)	241 (90)
V_d (mL)	2.78 (0.63)	30.5 (32)	2.97 (0.26)	4.36 (1.5)
V_{ss} (mL)	2.74 (0.46)	21.0 (18)	2.89 (0.24)	4.42 (1.2)
CL (mL/hr)	0.235 (0.03)	18.9 (4.5)	0.239 (0.05)	0.464 (0.17)
MRT (hr)	12.3 (2.2)	1.08 (0.99)	12.4 (1.9)	10.4 (3.9)

[a] $T_{1/2}$ = terminal biological half-life; AUC = total area under the blood concentration versus time curve; Vd = apparent volume of distribution; Vss = steady-state volume of distribution; CL = total body clearance; and MRT = mean residence time. Data are presented as mean and standard deviation (in parenthesis) (n = 8).

[b] W:W:W, weight ratio of DOX:PEG:HAuNS.